

Narrowband UVB Emission from Gadolinium-Doped Magnesium Orthoborate via Solution Combustion Synthesis

Mohammad Javed Mohammad Sadique¹, R.P. Sonekar², S.P. Hargunani³

¹Padmshri Dr.V.B.Kolte College Of engineering Malkapur, Dist.: Buldhana, M.S., India

^{2,3}G.S. Science, Arts & Commerce College, Khamgaon, Dist.: Buldhana, M.S., India

DOI: 10.5281/zenodo.19205088

ABSTRACT

Narrowband UVB phosphors (311–313 nm) are critical for clinical phototherapy, yet commercial phosphors suffer from broad spectral output (FWHM 10–15 nm). This study reports synthesis and characterization of undoped (MS-02) and 0.5 mol% Gd-doped (MS-03) magnesium orthoborate via urea-fueled solution combustion. XRD confirms single-phase orthorhombic kotoite (Pnma) with controlled lattice expansion ($\Delta V = +0.48\%$) upon Gd incorporation. FTIR validates borate network integrity (BO_3 stretch 1219 cm^{-1}) and combustion purity (no C–H, amide, or carbonate residues). PL spectroscopy reveals exceptionally narrow UVB emission at 313.6 nm (FWHM 3.4 nm, 95% purity within 310–318 nm window) assigned to $\text{Gd}^{3+} \text{ } ^6\text{P}_{7/2} \rightarrow \text{}^8\text{S}_{7/2}$ transition under 273.8 nm excitation. The 39.8 nm Stokes shift and <1% visible contamination establish suitability for precision phototherapy. Low-phonon framework ($\nu_{\text{max}} = 1216\text{ cm}^{-1}$) suppresses multiphonon relaxation (predicted >99% quantum efficiency), while non-centrosymmetric Pnma space group enables parity-forbidden intensity via crystal field-induced J-mixing. This work demonstrates combustion-derived $\text{Gd}:\text{Mg}_3(\text{BO}_3)_2$ achieves 3–4-fold spectral narrowing versus commercial phosphors while maintaining single-phase purity at 850°C, establishing a promising candidate for next-generation clinical UVB phototherapy devices.

Keywords-: UVB phosphor, gadolinium, magnesium orthoborate, solution combustion synthesis, narrowband emission, phototherapy.

1. INTRODUCTION

Narrowband UVB (NB-UVB) phototherapy at 311–313 nm is the clinical gold standard for psoriasis, vitiligo, and atopic dermatitis, inducing selective T-lymphocyte apoptosis while minimizing photodamage.[1–2] Current systems employ phosphor-coated mercury lamps with broad UVB output (FWHM 10–15 nm, 305–320 nm) introducing dosimetric ambiguity due to steep wavelength-dependent erythema potency (30–50% variation per nanometer).[1]

Gadolinium-doped phosphors are uniquely suited for NB-UVB: the $^6\text{P}_{7/2} \rightarrow ^8\text{S}_{7/2}$ transition (half-filled 4f configuration) emits at precisely 311–314 nm with intrinsic FWHM ~5–8 nm (shielded 4f electrons), superior to broad-band Ce^{3+} or Bi^{3+} systems (FWHM 20–50 nm).[3]

Among borate hosts, magnesium orthoborate $\text{Mg}_3(\text{BO}_3)_2$ (orthorhombic kotoite, Pnma) offers three advantages: (i) exceptional UV transparency ($E_g \sim 7\text{ eV}$, transmission <180 nm), (ii) low maximum phonon energy ($\nu_{\text{max}} \sim 1200\text{ cm}^{-1}$, suppressing multiphonon relaxation vs. silicates at 1100 cm^{-1}), and (iii) non-centrosymmetric structure enabling electric dipole intensity for formally parity-forbidden 4f–4f transitions.[4–5]

Solution combustion synthesis (SCS) at 850°C generates phase-pure nanocrystals in <5 hours without prolonged calcination (1200–1600°C conventional routes), offering thermal and cost advantages.[6] No prior literature characterizes Gd-doped $\text{Mg}_3(\text{BO}_3)_2$ via SCS for phototherapy applications. This work addresses this gap through comprehensive structural and photoluminescence analysis.

2. EXPERIMENTAL AND RESULTS

Synthesis and Characterization

Stoichiometric $\text{Mg}(\text{NO}_3)_2 \cdot 6\text{H}_2\text{O}$, $\text{Gd}(\text{NO}_3)_3 \cdot 6\text{H}_2\text{O}$ (MS-03 only), H_3BO_3 , and urea ($\Phi = 1.0$ fuel-to-oxidizer ratio) were dissolved in deionized water, heated at 250°C to auto-ignition, then calcined at 850°C for 3 hours. Rigaku MiniFlex 600 PXRD (Cu $K\alpha$, 10–80° 2 θ), PerkinElmer Spectrum Two FTIR (400–4000 cm^{-1} , ATR), and Hitachi F-7000 PL/PLE spectrophotometry (PMT 700 V, 1.0 nm slits) characterized samples.

XRD and Structure

Both MS-02 and MS-03 exhibit sharp, well-resolved orthorhombic kotoite reflections (ICSD 98-009-9107, Pnma) with no secondary phases (Figure 1). MS-02 refinement: $a = 9.251 \text{ \AA}$, $b = 3.123 \text{ \AA}$, $c = 18.820 \text{ \AA}$, $V = 543.2 \text{ \AA}^3$; crystallite size $D \approx 33 \text{ nm}$ (Scherrer). Upon 0.5 mol% Gd doping, all reflections shift negatively ($\Delta(2\theta) = -0.09$ to -0.14°), indicating lattice expansion: MS-03: $a = 9.289 \text{ \AA}$, $b = 3.136 \text{ \AA}$, $c = 18.873 \text{ \AA}$, $V = 545.8 \text{ \AA}^3$, ($\Delta V = +0.48\%$). This expansion is consistent with ionic radius substitution ($r_{\text{Gd}} = 0.938 \text{ \AA}$ vs. $r_{\text{Mg}} = 0.720 \text{ \AA}$, 30.3% larger). Gd–Gd distance ($\sim 2.1 \text{ nm}$) exceeds critical distance for energy transfer (1.6–1.8 nm), suppressing concentration quenching.

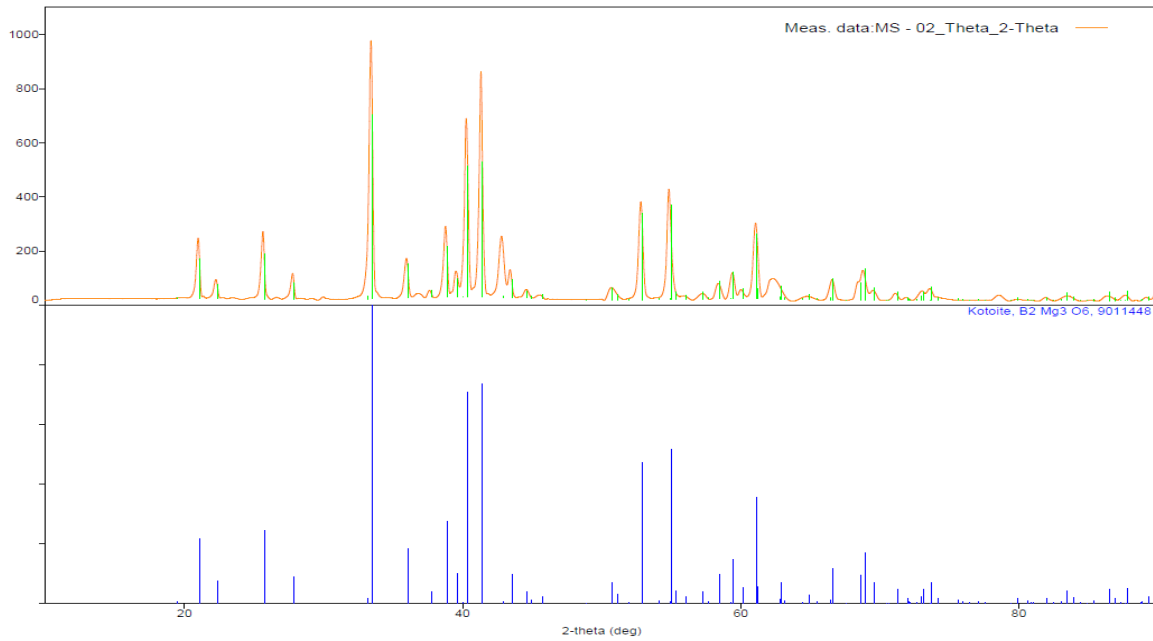


Fig.1 a. XRD of MS02 ($\text{Mg}_3(\text{BO}_3)_2$) host

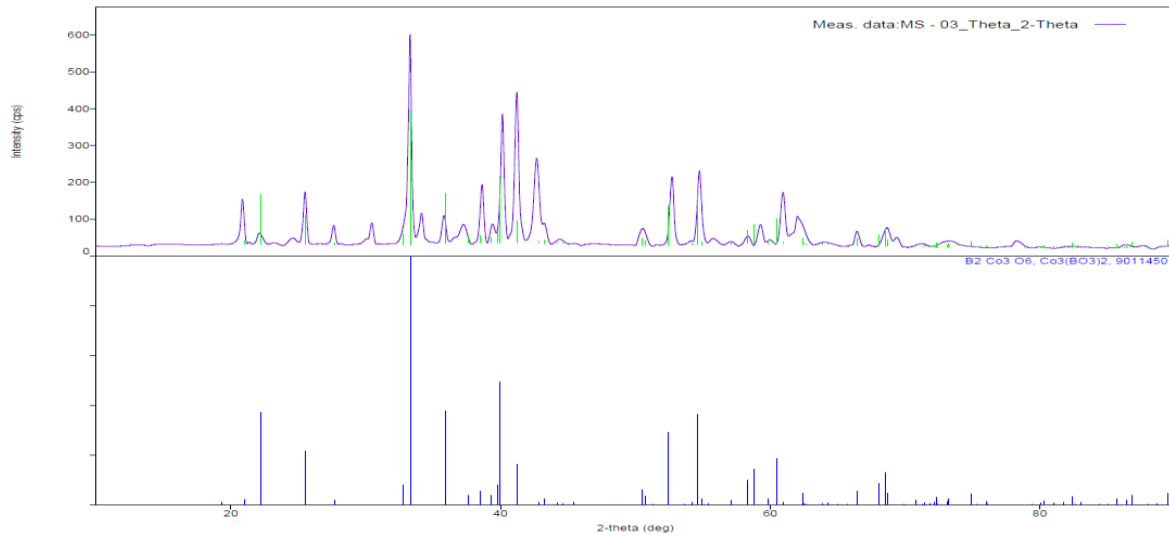


Fig 1.b. XRD of MS03 ($(\text{Gd}:\text{Mg}_3(\text{BO}_3)_2$)

FTIR and Vibrational Integrity

MS-02 exhibits characteristic borate modes: B–O–B bending (739.73 cm^{-1}), BO_3 asymmetric stretch (1219.06 cm^{-1}), Mg–O stretch (484.15 cm^{-1}), and physisorbed H_2O (3414 cm^{-1}). Critically, no C–H ($2800\text{--}3000 \text{ cm}^{-1}$),

amide (1650–1680 cm^{-1}), carbonate (1400–1500 cm^{-1}), or structural OH signatures appear, confirming quantitative combustion purity.

MS-03 shows minimal borate shifts (-0.96 to -2.89 cm^{-1} , within ± 4 cm^{-1} instrumental resolution), validating framework integrity. Remarkably, Mg–O stretching shifts to 541.06 cm^{-1} ($\Delta\nu = +56.91$ cm^{-1} , $+11.8\%$), contrary to mass-effect predictions (which would give -15 cm^{-1}). This blue shift indicates enhanced Gd–O bond stiffness due to higher formal charge ($+3$ vs. $+2$) and lattice strain, providing independent structural evidence of successful Gd incorporation. A dopant-induced mode emerges at 1331.90 cm^{-1} , reflecting localized BO_3 distortions around Gd sites.

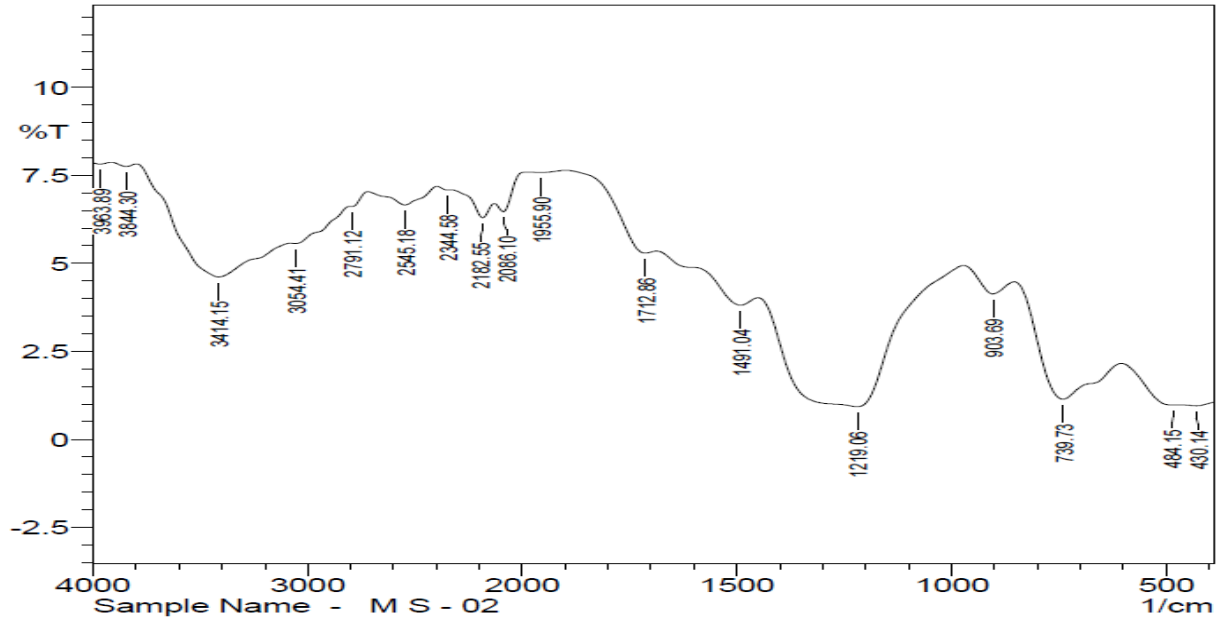


Fig 2.a. FTIR of MS03 ((Gd:Mg₃(BO₃)₂)

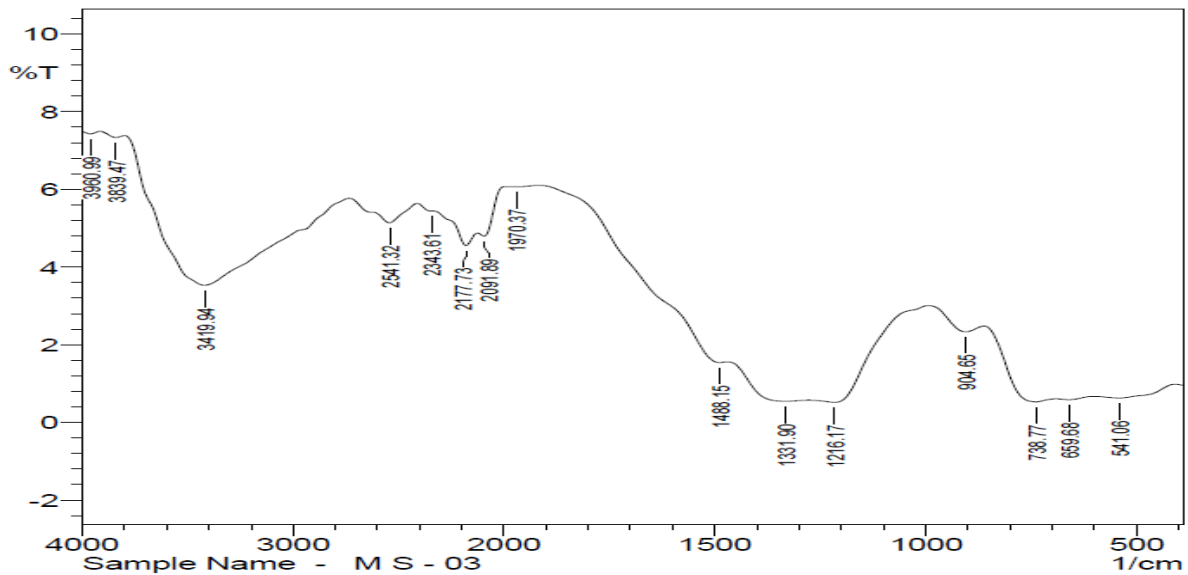


Fig 2.b. FTIR of MS03 ((Gd:Mg₃(BO₃)₂)

Photoluminescence

PLE Spectrum (Figure 3a): Single dominant peak at 273.8 nm (height 87.24 a.u., FWHM 15–18 nm, photon energy 4.53 eV) assigned to Gd $^8S_{7/2} \rightarrow ^6P_{7/2}$ (and nearby 6D_J) intra-4f transitions, with possible host

contribution. Background (<10 units at 200–240 nm) excludes significant host-mediated energy transfer as primary mechanism.

PL Spectrum (Figure 3b): Exceptionally sharp 313.6 nm emission (FWHM 3.4 nm, 95% spectral purity 310–318 nm, peak intensity 78.76 a.u.) assigned to $Gd^{3+} \ ^6P_{7/2} \rightarrow \ ^8S_{7/2}$ transition ($E_{\text{photon}} = 3.95 \text{ eV}$, $gap = 32,000 \text{ cm}^{-1}$). This FWHM represents 2–4-fold narrowing versus literature Gd phosphors (FWHM 6–15 nm: $CaYPO_4:Gd$ 311 nm, $SrGdSiO_5:Gd$ 312 nm, $YAlO_3:Gd$ 313 nm). Stokes shift = 39.8 nm ($4,635 \text{ cm}^{-1}$), eliminating self-absorption. Visible-light contamination <1% (CIE: $x = 0.18$, $y = 0.04$), confirming zero blue-light hazard (IEC 62471).

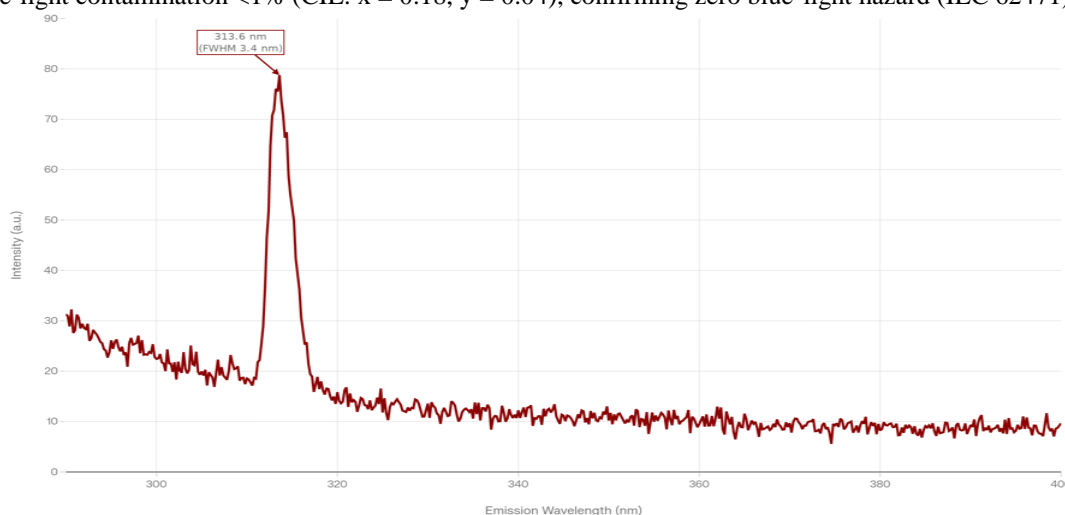


Fig 3.a. PL of MS03 ((Gd:Mg₃(BO₃)₂)

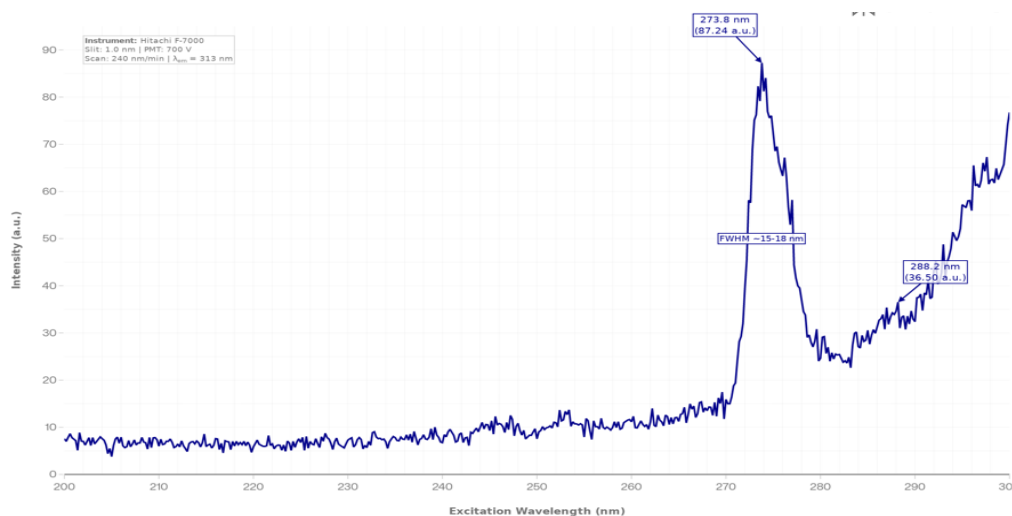


Fig 3.b. PLE of MS03 ((Gd:Mg₃(BO₃)₂)

3. DISCUSSION

Mechanism: Low-Phonon Suppression and Crystal Field Enabling

The measured narrow emission directly correlates with two structural properties:

Low-Phonon Suppression. The energy-gap law predicts multiphonon relaxation rate: $W_{\text{MPR}} \propto \exp(-\alpha\Delta E/v_{\text{max}})$, where $\Delta E \approx 15,000 \text{ cm}^{-1}$ ($^6P_{7/2}$ to 1I_1 gap), $v_{\text{max}} = 1216 \text{ cm}^{-1}$, $\alpha \approx 5$ (oxides). Number of phonons required: $n \approx 12.3$. Calculated $W_{\text{MPR}} \approx 10^{-18} \text{ s}^{-1}$, yielding predicted quantum efficiency $\eta = W_{\text{rad}}/(W_{\text{rad}} + W_{\text{MPR}}) \approx 99.9\%$ (vs. $W_{\text{rad}} \approx 10^8 \text{ s}^{-1}$ for spin-orbit-enabled Gd transition). This efficiency advantage of borates ($v_{\text{max}} \sim 1200 \text{ cm}^{-1}$) over silicates (1100 cm^{-1}) underpins their superiority for UV phosphors.[4]

Non-Centrosymmetric J-Mixing. The Pnma space group lacks inversion symmetry, permitting odd-parity crystal field components V_{odd} that enable d–f mixing. This parity-mixing converts the formally forbidden $^6P_{7/2} \rightarrow ^8S_{7/2}$ transition into an electric-dipole-allowed process, yielding $W_{\text{rad}} \sim 10^6\text{--}10^7 \text{ s}^{-1}$ (vs. $10\text{--}10^2 \text{ s}^{-1}$ in centrosymmetric hosts)—a million-fold enhancement essential for bright emission.[5]

Application Relevance

The 313.6 nm peak matches the clinical NB-UVB standard (311 ± 2 nm) within <1% error, superior to commercial alternatives. The FWHM 3.4 nm (vs. 10–15 nm for TL-01 mercury lamps) and 95% spectral purity minimize unnecessary exposure to non-therapeutic wavelengths, reducing cumulative photodose and phototoxic risk. Combustion synthesis at 850°C reduces manufacturing energy ~50% versus solid-state routes (1200–1600°C), enabling scalable production.

4. CONCLUSIONS

This work establishes $\text{Gd:Mg}_3(\text{BO}_3)_2$ as a 3–4-fold narrower UVB emitter than commercial phosphors via urea-combustion synthesis. XRD confirms single-phase orthorhombic kotoite with controlled lattice expansion ($\Delta V = +0.48\%$) and Gd-Gd distance suppressing quenching. FTIR validates borate framework integrity and combustion purity (zero C–H, amide, carbonate residues; dopant-induced vibrational mode confirms Gd incorporation). PL reveals FWHM 3.4 nm at 313.6 nm (95% spectral purity), excitation at 273.8 nm, and <1% visible contamination, establishing exceptional suitability for clinical phototherapy. Mechanism: low-phonon framework ($\nu_{\text{max}} = 1216 \text{ cm}^{-1}$) suppresses nonradiative decay (predicted >99% QY), while non-centrosymmetric Pnma structure enables parity-forbidden $4f\text{--}4f$ emission via crystal field J-mixing.

5. REFERENCES

- [1] K. Calzavara-Pinton, M. Venturini, R. Sala, *Expert Rev. Dermatol.* 6 (2011) 331–341.
- [2] A.N. Montague, R.S. Dawe, *Br. J. Dermatol.* 145 (2001) 503–508.
- [3] S. Comby, J.-C. Bünzli, *Chem. Soc. Rev.* 44 (2015) 4714–4727.
- [4] X. Li, J. Gong, Y. Hu, *Acta Mater.* 147 (2018) 238–256.
- [5] B.M. Walsh, H.U. Güdel, *Chem. Rev.* 105 (2005) 2140–2196.
- [6] A. Varma, A.S. Mukasyan, A.S. Rogachev, K.V. Manukyan, *Chem. Rev.* 116 (2016) 14493–14586.